



Pressure effect on structural and vibrational properties of Sm-substituted BiFeO₃

Yu-Jie Wu, Xiao-Kun Chen, Jing Zhang, Jing Liu, Wan-Sheng Xiao, Zhigang Wu, and Xiao-Jia Chen

Citation: *Journal of Applied Physics* **114**, 154110 (2013); doi: 10.1063/1.4826069

View online: <http://dx.doi.org/10.1063/1.4826069>

View Table of Contents: <http://scitation.aip.org/content/aip/journal/jap/114/15?ver=pdfcov>

Published by the [AIP Publishing](#)

Advertisement:



Re-register for Table of Content Alerts

Create a profile.



Sign up today!



Pressure effect on structural and vibrational properties of Sm-substituted BiFeO₃

Yu-Jie Wu,^{1,2} Xiao-Kun Chen,¹ Jing Zhang,¹ Jing Liu,³ Wan-Sheng Xiao,⁴ Zhigang Wu,⁵ and Xiao-Jia Chen^{1,6,a)}

¹Department of Physics, South China University of Technology, Guangzhou 510640, China

²School of Physics and Electronic Engineering, Guangzhou University, Guangzhou 510006, China

³Institute of High Energy Physics, Chinese Academy of Sciences, Beijing 100190, China

⁴Guangzhou Institute of Geochemistry, Chinese Academy of Sciences, Guangzhou 510640, China

⁵Department of Physics, Colorado School of Mines, Golden, Colorado 80401, USA

⁶Center for High Pressure Science and Technology Advanced Research, Shanghai 201203, China

(Received 5 February 2013; accepted 2 October 2013; published online 17 October 2013)

The structural and vibrational properties of 5% Sm-substituted BiFeO₃ under pressure are investigated using synchrotron X-ray diffraction and Raman scattering measurements. The results yield the pressure-induced structural phase transitions from the polar R3c phase to the orthorhombic Pnma phase commencing at 3.9 and being complete at 7.6 GPa, where there is a region of the coexistence of the R3c and Pnma phases. This structural transition is accompanied by the ferroelectric-paraelectric transition for the Sm-substituted BiFeO₃. We find that the Sm substitution leads to lower transition pressure compared to that of the pure BiFeO₃ system due to the substitution-induced chemical pressure. Our results do not suggest the pressure-induced reentrance of ferroelectricity in the model multiferroic BiFeO₃ in the pressure range studied. © 2013 AIP Publishing LLC.

[<http://dx.doi.org/10.1063/1.4826069>]

I. INTRODUCTION

Multiferroics, in particular those exhibit both magnetic order and ferroelectricity in the same phase, have recently drawn renewed interest because of their intriguing properties and great potential for new types of magnetoelectric devices.^{1–4} Among these multiferroic materials, BiFeO₃ (BFO) is most attractive because of its high ferroelectric Curie temperature $T_C = 1103$ K and the antiferromagnetic Néel temperature $T_N = 643$ K, both well above room temperature.⁵ The main impetus for ferroelectricity in BiFeO₃ comes from the stereo-chemically active 6s² lone pair of Bi³⁺, while its magnetic structure is of G-type with a cycloid spiral arrangement of magnetic moments of Fe³⁺ ions. However, BiFeO₃ suffers from high-leakage current and large coercive fields, as well as small electromechanical coefficients. It has been shown that some of such shortcomings can be overcome by substituting rare-earth Sm³⁺ ions for A-sites of the BiFeO₃ perovskite cell.⁶ The subtle modifications in atomic composition can induce lattice distortion, and hence the functional behaviors of the parent ferroelectric perovskite could be tuned.

Besides being a model multiferroic, BiFeO₃ is also one of the very few perovskites that present both octahedral tilts and strong ferroelectric cation displacements at room temperature.⁷ Under high pressures, these competing properties will be altered to different extent. In order to characterize the structural, magnetic, and ferroelectric properties of BiFeO₃ under high pressures, numerous experimental and theoretical works have been performed.^{8–11} In spite of such extensive

investigations using a variety of techniques, many controversies still remain.

First-principles calculations⁸ based on the density functional theory (DFT) have predicted a pressure-induced phase transition from the rhombohedral (*R3c*) phase to the orthorhombic (*Pnma*) phase in BiFeO₃ around 13 GPa. Experimentally, Yang *et al.*¹² reported that three structural transitions took place at around 3, 8.6, and 44.6 GPa using Raman spectroscopy, while Gavriluk *et al.*¹³ found no phase transitions below 50 GPa with synchrotron X-ray powder diffraction. However, they found the effect of magnetic collapse in a pressure range of 45–55 GPa using nuclear forward scattering and X-ray emission spectroscopy^{14,15} and discussed the “Hubbard energy control” mechanism of the effect.¹⁶ Besides, the magnetic behavior was completely reversible.¹⁷ Belik *et al.*¹⁸ suggested the sequence of the phase transitions on compression: rhombohedral *R3c* → Orthorhombic I → Orthorhombic II → Orthorhombic *Pnma* → cubic. However, Haumont *et al.*¹⁹ observed only two phase transitions around 3.5 and 10 GPa, respectively, corresponding to *R3c* → *C2/m* → *Pnma*. A very recent single-crystal X-ray and Raman spectroscopy study⁷ reveals that BFO undergoes a surprising richness of six phase transitions up to 55 GPa, and a structural phase transition²⁰ from the polar rhombohedral *R3c* phase to the orthorhombic *Pbam* phase with anti-ferroelectric atomic displacements was discovered by neutron diffraction technique at 3 GPa. In addition, Gavriluk *et al.*¹⁰ observed an insulator-metal transition through resistance measurements. Therefore, further investigations on the structural and physical properties of BiFeO₃ under high pressures are in crucial need, especially by combining both the chemical and physical pressures.

^{a)}Author to whom correspondence should be addressed. Electronic mail: xjchen@ciw.edu

In this paper, we present synchrotron X-ray diffraction and Raman scattering investigations of 5%-Sm-substituted BiFeO_3 under pressures up to 13.4 GPa and 21.6 GPa, respectively. Prominent changes in the X-ray data and the Raman spectra indicate a structural transformation from the $R3c$ rhombohedral symmetry to the orthorhombic $Pnma$ phase at around 7.6 GPa, accompanying with the ferroelectric-paraelectric transition under the combined action of the chemical and physical pressures. Before the transformation, the system is in the coexisted $R3c$ and $Pnma$ phases. Our results provide further information for understanding the coupling between the structure and other properties of BiFeO_3 under the coactions of the chemical and physical pressures.

II. EXPERIMENTS

$\text{Bi}_{0.95}\text{Sm}_{0.05}\text{FeO}_3$ powders were synthesized via a modified wet chemical method. Stoichiometric amounts of $\text{Bi}(\text{NO}_3)_3 \cdot 5\text{H}_2\text{O}$, $\text{Fe}(\text{NO}_3)_3 \cdot 9\text{H}_2\text{O}$, and $\text{Sm}(\text{NO}_3)_3 \cdot 6\text{H}_2\text{O}$ were dissolved in dilute nitric acid, and calculated amounts of tartaric acid were added as a complexing agent. The resultant solution was evaporated and dried at 150°C with stirring to obtain xerogel powders. Then the xerogel powders were grinded in an agate mortar. The obtained powders were preheated to 300°C for 1 h in order to remove excess hydrocarbons and NO_x impurities. Finally, all samples were further annealed at 600°C for 2 h. The $\text{Bi}_{0.95}\text{Sm}_{0.05}\text{FeO}_3$ powder belongs to a single-phase rhombohedral $R3c$ structure examined by x-ray powder diffraction (XRD) at ambient pressure.

The *in situ* high-pressure synchrotron x-ray diffraction (SXRD) measurements were performed at the Beijing Synchrotron Radiation Facility using a symmetry diamond anvil cell. A monochromatic x-ray beam with a wavelength of 0.6199 \AA was used. The culet size of the diamond anvil was $350 \mu\text{m}$ in diameter. A $300 \mu\text{m}$ thick steel gasket (T301) was preindented to $30 \mu\text{m}$ thickness ($120 \mu\text{m}$ initial hole diameter). The mixture of methanol and ethanol (4:1) as pressure-transmitting medium was injected into the chamber to ensure better quasihydrostatic pressure condition. The fluorescence of ruby was used as a pressure gauge.²¹ These vibrational modes at high-pressure were measured by Raman scattering technique. The spectra were recorded on a spectrometer with a low-frequency cut off at 100 cm^{-1} . The exciting laser line was the He-Ne at the 532 nm laser line. The laser power was kept at 10 mW on the diamond anvil cell to avoid heating of the sample. Before measuring the pressure, the sample was stewing for half an hour after pressurized. We measured the pressure just before and after accumulation of x-ray and Raman patterns from the sample. The pressure given is the average value of the two pressures.

III. RESULTS AND DISCUSSION

We have performed a structural study of $\text{Bi}_{0.95}\text{Sm}_{0.05}\text{FeO}_3$ at high pressures up to 13.4 GPa. Figure 1 shows the diffraction patterns at various pressures. Even though pressure could bring about the rhombohedral distortion and peak splitting, we clearly observed the $R3c$ phase below 4.1 GPa. With increasing

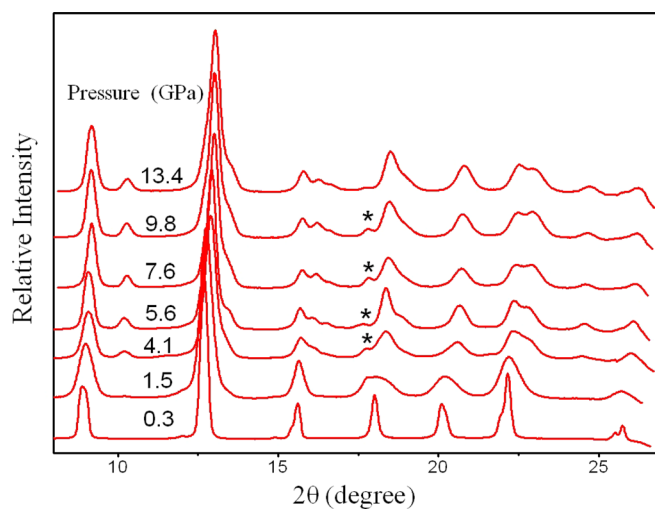


FIG. 1. Synchrotron X-ray powder diffraction patterns of $\text{Bi}_{0.95}\text{Sm}_{0.05}\text{FeO}_3$ at various pressures and room temperature. Star * indicates diffraction peak from the metal gasket.

pressure, we also observed significant changes in the multiplicity and intensity of the Bragg peaks. Specifically at pressure of 4.1 GPa, a new peak is observed at an angle $2\theta \approx 10^\circ$, and the intensities of the peaks at around 16° suddenly become weak, indicating the appearance of a new phase.¹⁹

In order to get more details about structural properties, we simulated the measured SXRD patterns of the samples based on the Le Bail method by the GSAS program. Figure 2 displays three selected diffraction patterns of $\text{Bi}_{0.95}\text{Sm}_{0.05}\text{FeO}_3$ at 0.3, 4.1, and 9.8 GPa corresponding to the three different phases regions, respectively. As expected, the low-pressure phase at 0.3 GPa is well described using the $R3c$ rhombohedral

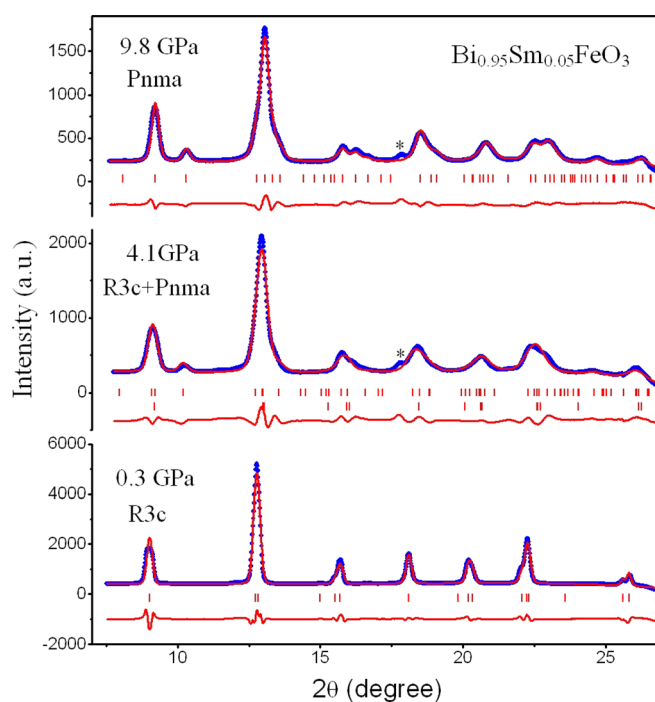


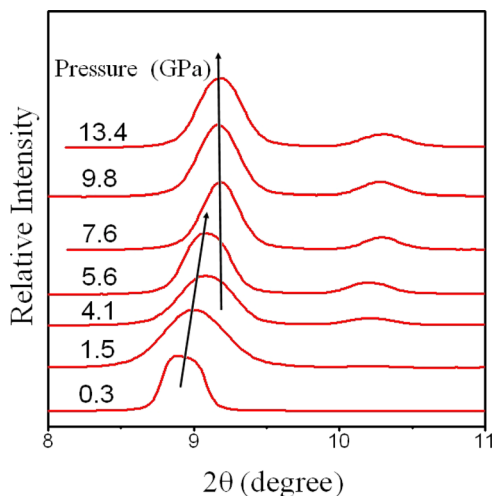
FIG. 2. Refinement diffraction patterns of $\text{Bi}_{0.95}\text{Sm}_{0.05}\text{FeO}_3$ at three selected pressures (0.3, 4.1, and 9.8 GPa) representing rhombohedral $R3c$ phase, coexistence of $R3c$ and $Pnma$, orthorhombic $Pnma$ phase symmetries, respectively. Star * indicates diffraction peak from the metal gasket.

TABLE I. The indexation of the diffraction lines of $\text{Bi}_{0.95}\text{Sm}_{0.05}\text{FeO}_3$ at 0.3 GPa.

2theta (deg)	d (Å)	H	K	L
9.0	3.94	0	1	2
12.8	2.78	1	1	0
14.9	2.38	1	1	3
15.5	2.29	0	0	6
15.7	2.27	2	0	2
18.1	1.98	0	2	4
20.2	1.77	1	1	6
22.1	1.62	0	1	8
22.3	1.60	3	0	0
25.6	1.40	2	0	8
25.8	1.39	2	2	0

symmetry, and the indexation of the diffraction lines at 0.3 GPa is given in Table I. The unit-cell parameters measured at ambient conditions are $a = b = 5.567(1)$ Å and $c = 13.819(8)$ Å (hexagonal setting), in good agreement with the reported values in literature.²² With increasing pressure, a new phase is evidenced from the appearance of some reflections in the diffraction pattern (Figure 1). For example, a typical reflection (111), which could be attributed to the orthorhombic *Pnma* phase, was observed in the present profile at 4.1 GPa. However, the fit at 4.1 GPa was significantly improved when including two phases *R3c* + *Pnma* ($\chi^2 = 1.12$) instead of a single phase ($\chi^2 = 1.44$ for *Pnma*). The similar phenomenon was also observed for the data at 5.7 GPa. The former two-phase model always yields better agreement between the experimental and theoretical spectra, thus indicating that the crystal structures at 4.1 and 5.7 GPa are characterized by the coexistence of *R3c* and *Pnma*, which can be seen clearly in Fig. 3. The single orthorhombic *Pnma* structure appears above 7.6 GPa, as shown in Figs. 1 and 3.

Figure 4 shows the pressure dependence of the lattice parameters of the $\text{Bi}_{0.95}\text{Sm}_{0.05}\text{FeO}_3$ sample, expressed in a pseudocubic cell. In the low-pressure region, the rhombohedral phase is very sensitive to pressure as we observed a significant decrease in a_R and c_R . The second phase,

FIG. 3. Fragment (from 8 to 11° in 2θ) of synchrotron X-ray powder diffraction patterns of $\text{Bi}_{0.95}\text{Sm}_{0.05}\text{FeO}_3$ at room temperature.

orthorhombic *Pnma*, appears at 4.1 GPa. The coexistence of *R3c* and *Pnma* in the pressure range from 3.9 to 7.5 GPa corresponds to the change of the cation-anion displacement and the appearance of the tilting of the octahedral.¹² At higher pressures, the structure transition from *R3c* to *Pnma* for $\text{Bi}_{0.95}\text{Sm}_{0.05}\text{FeO}_3$ completes at 7.6 GPa. It has been established that substitution could serve as chemical pressure due to the smaller ionic radius of Sm^{3+} (1.28 Å) compared to Bi^{3+} (1.36 Å). The pressure effect on multiferroics in $\text{Bi}_{0.95}\text{Sm}_{0.05}\text{FeO}_3$ benefited the lattice modification, which made the phase transition from the rhombohedral *R3c* to the orthorhombic *Pnma* to occur earlier than those in the unsubstituted system reported previously.^{11,12,19}

To reveal the compressibility of each phase, we plot the pressure dependence of the volume per formula unit, expressed in a pseudocubic cell, in Fig. 5. Under pressure, the volume of the unit cell was compressed, consequently leading to the reduction of the tilting of octahedral in the phase coexistence region of *R3c* and *Pnma*.¹² A large volume drop was observed at the transition pressure, which indicated the first order feature of the pressure-induced phase transition of $\text{Bi}_{0.95}\text{Sm}_{0.05}\text{FeO}_3$. The unit cell volumes (V) of the two phases as a function of pressure (P) were fitted with the third order Birch-Murnaghan equation of states

$$P = 3K_0 f_E (1 + 2f_E)^{5/2} \left[1 + \frac{3}{2} (K'_0 - 4) f_E \right],$$

where $f_E = [(V_0/V)^{2/3} - 1]/2$, V_0 is the volume at ambient pressure, V is the volume at pressure P given in GPa, K_0 is the bulk modulus, and K'_0 is the first pressure derivative of K_0 . The solid lines in Fig. 5 represent the fitted results. In the low pressure *R3c* phase, the bulk modulus K_0 is 132 ± 20 GPa with $K'_0 = 3.5 \pm 0.5$, $V_0 = 61.7 \pm 0.2$ Å³. The value of K_0 is much larger than that of the pure BiFeO_3 .¹⁰ It indicates that $\text{Bi}_{0.95}\text{Sm}_{0.05}\text{FeO}_3$ is harder than pure BiFeO_3 at the low pressure, which benefits the lattice modification by Sm substitution. In the high-pressure *Pnma* phase, $V_0 = 59.7 \pm 0.4$ Å³, $K_0 = 257 \pm 48$ GPa, $K'_0 = 3.3 \pm 0.6$. The bulk modulus value matches well with that of the pure BiFeO_3 in the high-pressure phase,¹⁰ signaling the almost same compressibility of $\text{Bi}_{0.95}\text{Sm}_{0.05}\text{FeO}_3$ and BiFeO_3 at high pressures. This indicates that the chemical pressure effect vanishes at high pressures in doped BiFeO_3 .

The structural transition of $\text{Bi}_{0.95}\text{Sm}_{0.05}\text{FeO}_3$ under pressure is similar to that of BiFeO_3 upon rare-earth ion substitution at A-site.²³ The ferroelectric property is closely related to the structural transformation. The rhombohedral *R3c* symmetry characterized by the anti-phase octahedral tilting and off-center cation displacements displays ferroelectricity,²⁴ while the high-pressure *Pnma* symmetry exhibiting²⁵ is in favor of paraelectricity. Thus, the coexisting region should include a competition between ferroelectricity and paraelectricity. According to DFT calculations, a pressure-induced phase transition from the rhombohedral *R3c* to the orthorhombic *Pnma* symmetry in BiFeO_3 is expected to be observed at 13 GPa,⁸ which is in good agreement with experiments. For instance, Haumont *et al.*¹⁹ observed the nonpolar orthorhombic *Pnma* structure in BiFeO_3 above

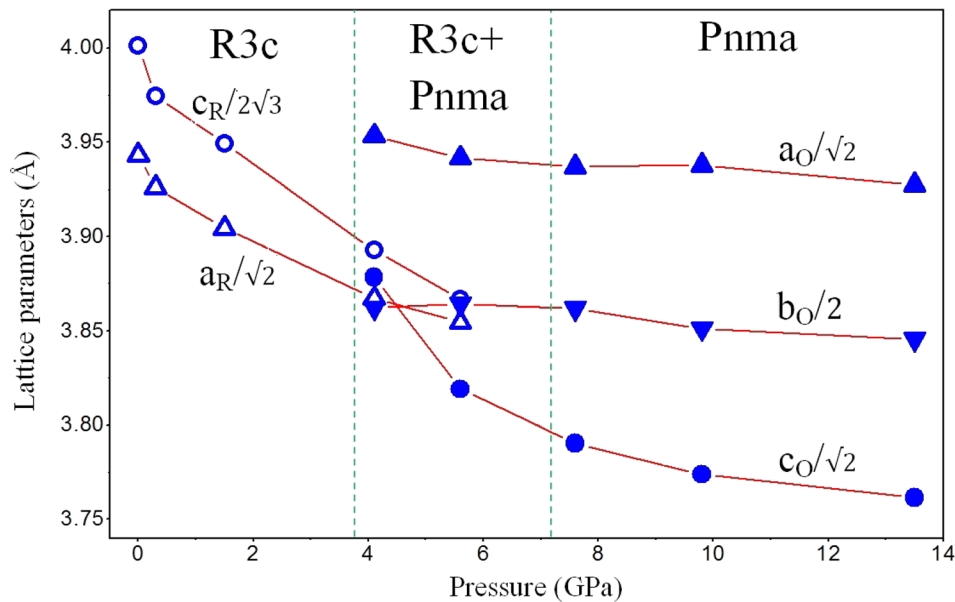


FIG. 4. The pressure dependence of the normalized lattices parameters of $\text{Bi}_{0.95}\text{Sm}_{0.05}\text{FeO}_3$. The cell parameters are described in a pseudocubic cell $a_{pc} = a/\sqrt{2}$ and $c_{pc} = c/2\sqrt{3}$ for the $R3c$ phase, $a_{pc} = a/\sqrt{2}$, $b_{pc} = b/2$, and $c_{pc} = c/\sqrt{2}$ for the $Pnma$ phase.

10 GPa through the far-IR reflectively measurement; at 11 GPa, Guennou *et al.*⁷ observed the transition to the $Pnma$ phase by changes in both the diffraction patterns and the Raman signature. Our measured transition pressure for Sm-substituted BFO is much lower than that in pure BFO because of the chemical pressure, which results from the reduced lattices due to the smaller ionic radius of Sm^{3+} compared to Bi^{3+} .

Raman spectroscopy has been demonstrated to be a very useful technique in studying phase transitional characteristics and local structure modulation in ferroelectric materials.^{11,26} The Raman active modes of BiFeO_3 with the space group $R3c$ at room temperature can be written as $\Gamma = 4A_1 + 9E$,²⁷ while the Raman modes in the orthorhombic phase with the space group $Pnma$ can be described by $\Gamma = 7A_g + 5B_{1g} + 7B_{2g} + 5B_{3g}$.²⁸ Figure 6 shows pressure-dependent Raman spectra of $\text{Bi}_{0.95}\text{Sm}_{0.05}\text{FeO}_3$ in the range from atmospheric

pressure to 21.6 GPa, indicating that the Raman signature (thus the structure) undergoes some significant changes. The phonon mode assignment at pressures below 4.3 GPa was made by comparing the spectra for the pure BiFeO_3 with that for space group $R3c$.^{29,30} At the ambient conditions, the peaks of $\text{Bi}_{0.95}\text{Sm}_{0.05}\text{FeO}_3$ sample at 142.6, 173.1, 230.2, and 436.0 cm^{-1} correspond to A_1 (TO) modes, and the other peaks at 126.0, 262.6, 278.3, 299.1, 341.7, 368.4, 472.0, 527.7, and 618.3 cm^{-1} are the E (TO) modes, respectively. In the low-pressure range below 4.3 GPa, the Raman peaks shift to higher frequency gradually with increasing pressure. This phenomenon is due to the pressure-induced bond shortening and lattice distortion. It is interesting to note that a new peak at around 213.6 cm^{-1} , which points to a structural reordering, appears at the pressure of 4.3 GPa, and the intensity of the A_1 (TO) mode at around 436.0 cm^{-1} increases suddenly at 4.3 GPa. When pressure is increased to 8.2 GPa,

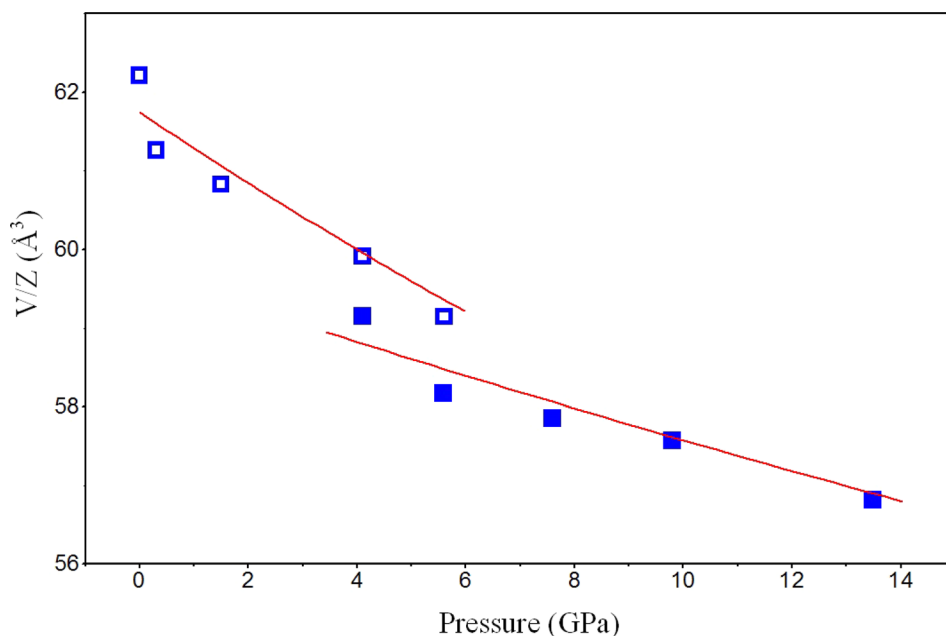


FIG. 5. The pressure dependence of unit cell volume divided by the number of formula units per unit cell Z of $\text{Bi}_{0.95}\text{Sm}_{0.05}\text{FeO}_3$. The solid lines demonstrate the fitting data of phase to the Birch-Murnaghan equation of state.

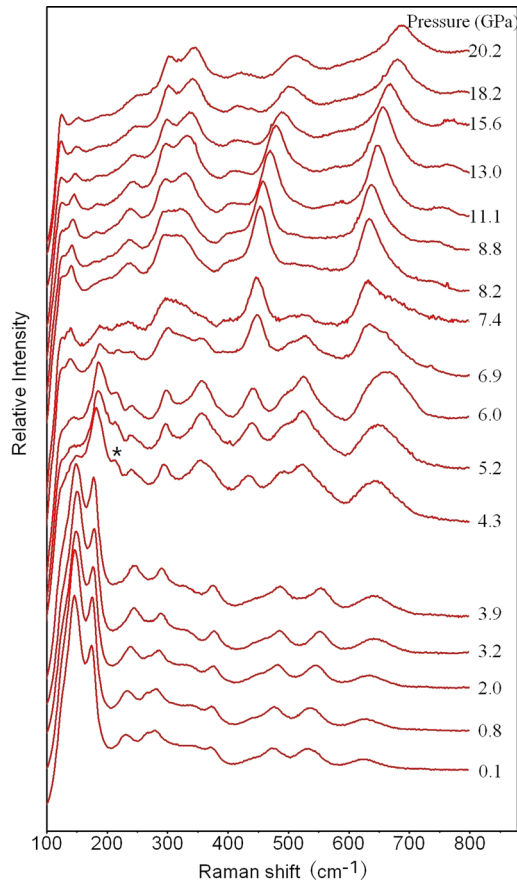


FIG. 6. Raman scattering spectra of $\text{Bi}_{0.95}\text{Sm}_{0.05}\text{FeO}_3$ for several selected pressures at room temperature. Star * marks the position of the phonon mode at 213.6 cm^{-1} emerging at 4.3 GPa.

the two E (TO) modes at around 472.0 and 527.7 cm^{-1} disappear.

In accordance with our structural studies, we present the pressure dependence of the Raman frequencies of different modes for $\text{Bi}_{0.95}\text{Sm}_{0.05}\text{FeO}_3$ in Fig. 7. Two conspicuous spectral features can be seen clearly. First, a new Raman

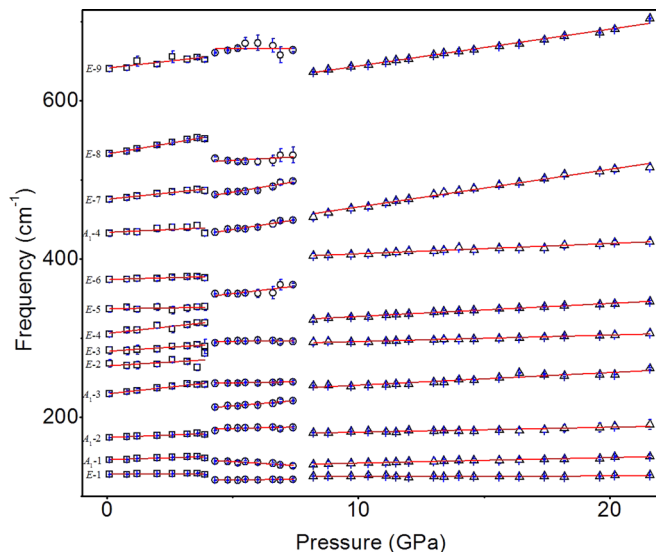


FIG. 7. The pressure dependence of the frequencies of the Raman modes for $\text{Bi}_{0.95}\text{Sm}_{0.05}\text{FeO}_3$.

peak appears at around 4.3 GPa, indicating a new phase at the pressure range of 3.9 to 4.3 GPa, but the characteristic peaks of $R3c$ phase still maintain in the pressure range from 4.3 to 7.4 GPa, corresponding to the coexistence of $R3c$ and $Pnma$ phases. At higher pressure, the phase transition is indicated by the disappearance of the two E (TO) modes at around 472.0 and 527.7 cm^{-1} at pressure of 8.2 GPa. We assign the space group $Pnma$ to the orthorhombic phase at this pressure region, even though we only observed 9 out of 24 Raman modes that the $Pnma$ symmetry should give. The independent scattering configurations can only be obtained with the polarizations measurement owing to the x and z directions. These configurations are indistinguishable in $Pnma$ phase. Therefore, in the case of unpolarized measurements using a powdered sample, the number of the observed Raman modes in the $Pnma$ perovskite is usually about less than half of the predicted number of 24.^{12,31}

It is well known that the Grüneisen parameter γ plays a crucial role in understanding the thermodynamic and thermoelastic behavior of solids. The slopes of phonon frequency versus pressure curves are calculated according to the results displayed in Fig. 7. Table II summarizes the ambient-pressure phonon frequencies ω_{0i} , their pressure derivatives $d\omega_i/dP$ and mode Grüneisen parameters γ_i for both phases of $\text{Bi}_{0.95}\text{Sm}_{0.05}\text{FeO}_3$. The Grüneisen parameters for the low and high pressure phases were calculated using the formula

$$\gamma_i = (K_0/\omega_{0i})(d\omega_i/dp),$$

where K_0 and ω_{0i} are the bulk modulus and the ambient-pressure phonon frequencies, respectively. The bulk modulus obtained from the synchrotron X-ray data is 132 GPa for the rhombohedral phase and 257 GPa for the orthorhombic phase, respectively. The $d\omega_i/dP$ and the orthorhombic phase ω_{0i} come from the linear fitting results as described in Fig. 6. According to the expression of Grüneisen parameters, γ_i is in direct proportion to the

TABLE II. The ambient-pressure phonon frequencies ω_{0i} (in cm^{-1}), pressure derivatives of frequencies $d\omega_i/dp$ (in $\text{cm}^{-1}\text{ GPa}^{-1}$), and Grüneisen parameters γ_i for various Raman modes of $\text{Bi}_{0.95}\text{Sm}_{0.05}\text{FeO}_3$ in low-pressure and high-pressure phases.

Mode	Low-pressure (rhombohedral) phase			High-pressure (orthorhombic) phase		
	ω_{0i}	$d\omega_i/dp$	γ_i	ω_{0i}	$d\omega_i/dp$	γ_i
$E-1$	126.0	0.13	0.14	124.9	0.03	0.07
A_{1-1}	142.6	0.93	0.86	140.0	0.70	1.28
A_{1-2}	173.1	1.21	0.93	180.3	0.62	0.87
A_{1-3}	230.2	3.43	1.97	239.9	1.59	1.70
$E-2$	262.6	1.92	0.97			
$E-3$	278.3	2.01	0.96	294.5	0.82	0.72
$E-4$	299.1	3.43	1.51	323.0	1.65	1.31
$E-5$	341.7	0.42	0.16			
$E-6$	368.4	0.88	0.31	404.0	1.31	0.83
A_{1-4}	436.0	1.45	0.44	453.1	4.76	2.70
$E-7$	472.0	3.30	0.93			
$E-8$	527.7	5.44	1.36			
$E-9$	618.3	3.56	0.76	635.7	4.66	1.89

$d\omega_i/dP$, suggesting that the bigger the pressure derivative of ω_i is, the larger γ_i is. The Grüneisen parameters γ_i for the lower pressure phase in the $\text{Bi}_{0.95}\text{Sm}_{0.05}\text{FeO}_3$ are much smaller than those in BiFeO_3 ,¹² indicating again the benefit from the lattice modification provided by the chemical pressure. Since the Grüneisen parameters in $\text{Bi}_{0.95}\text{Sm}_{0.05}\text{FeO}_3$ are always smaller than those of parent BiFeO_3 , shifting of the transition pressure to lower pressure region is expected.

As given in Table II, in the lower pressure range, γ_{A_1-3} and γ_{E-4} are much bigger than that of other modes. This is consistent with the results presented in Fig. 7, in which the frequency blueshift rates for A_1-3 and $E-4$ modes are larger than those for other modes. Moreover, the slopes of $d\omega_i/dP$ for the mode below 350 cm^{-1} in the higher pressure range are much smaller than those in the lower pressure range, while the slopes of $d\omega_i/dP$ for the modes over 350 cm^{-1} have a different variation tendency. The abrupt changes in the slopes of $d\omega_i/dP$ and Grüneisen parameters γ_i provide the evidence of the rhombohedral-orthorhombic phase transition.

In “conventional” ferroelectric materials, pressure can reduce even annihilate ferroelectricity. This behavior can be understood by recalling that external pressure modifies the delicate balance between long-range Coulomb interactions and short-range electronic forces, favoring, respectively, ferroelectric distortions and a paraelectric cubic structure.³² However, unexpectedly, further dramatically increasing pressure could induce ferroelectricity again, which is different in nature from conventional ferroelectric behaviors. This is because the high-pressure ferroelectricity is driven by an original electronic effect rather by long-range interactions.^{33–35} In $\text{Bi}_{0.95}\text{Sm}_{0.05}\text{FeO}_3$, the ferroelectric-paraelectric transitions have been observed, but we did not find any evidence of the pressure-induced reentrance of ferroelectricity. Instead, a nonpolar orthorhombic structure has been observed at high pressures we applied. Although strongly correlated electronic effect might play an important role on ferroelectricity in BFO systems, further increasing pressure is required to examine if such reappearance of ferroelectricity would eventually occur.

IV. CONCLUSIONS

We have investigated the structural and vibrational properties of $\text{Bi}_{0.95}\text{Sm}_{0.05}\text{FeO}_3$ under pressure in a diamond-anvil cell up to 13.4 and 21.6 GPa, respectively, using the synchrotron X-ray diffraction and Raman spectroscopy, and we find that pressure induces a structural transition from the polar $R3c$ phase to the nonpolar orthorhombic $Pnma$ phase commencing at 3.9 and being complete at 7.6 GPa. The transition occurs through an obvious coexistence of these two phases, corresponding to a ferroelectric-paraelectric sequence. Moreover, the paraelectric orthorhombic $Pnma$ structure remains stable over the pressure range of 8.3 to 21.6 GPa, and the stability of this phase at higher pressures remains an interesting research topic.

ACKNOWLEDGMENTS

We acknowledge the Beijing Synchrotron Radiation Facility (BSRF) for the provision of beam time. This work

was supported by the Cultivation Fund of the Key Scientific and Technical Innovation Project, Ministry of Education of China (No. 708070), the Fundamental Research Funds for the Central Universities SCUT (No. 2012zz0078), and the National Natural Science Foundation of China (Nos. 10874046 and 11104081). Z.W. acknowledges the U.S. DOE early career research award (No. DE-SC0006433).

- ¹R. Ramesh and N. A. Spaldin, *Nat. Mater.* **6**, 21 (2007).
- ²S.-W. Cheong and M. Mostovoy, *Nat. Mater.* **6**, 13 (2007).
- ³H. Béa, M. Gajek, M. Bibes, and A. Barthélémy, *J. Phys.: Condens. Mater.* **20**, 434221 (2008).
- ⁴G. Catalan and J. F. Scott, *Adv. Mater.* **21**, 2463 (2009).
- ⁵A. M. Kadomtseva, Y. F. Popov, A. P. Pyatakov, G. P. Vorob'ev, A. K. Zvezdin, and D. Viehland, *Phase Trans.* **79**, 1019 (2006).
- ⁶C. J. Cheng, D. Kan, S. H. Lim, W. R. McKenzie, P. R. Munroe, L. G. SalamancaRiba, R. L. Withers, I. Takeuchi, and V. Nagarajan, *Phys. Rev. B* **80**, 014109 (2009).
- ⁷M. Guennou, P. Bouvier, G. S. Chen, B. Dkhil, R. Haumont, G. Garbarino, and J. Kreisel, *Phys. Rev. B* **84**, 174107 (2011).
- ⁸P. Ravindran, R. Vidya, A. Kjekshus, and H. Fjellvag, *Phys. Rev. B* **74**, 224412 (2006).
- ⁹D. H. Wang, L. Yan, C. K. Ong, and Y. W. Du, *Appl. Phys. Lett.* **89**, 182905 (2006).
- ¹⁰A. G. Gavriliuk, V. V. Struzhkin, I. S. Lyubutin, S. G. Ovchinnikov, M. Y. Hu, and P. Chow, *Phys. Rev. B* **77**, 155112 (2008).
- ¹¹R. Haumont, J. Kreisel, and P. Bouvier, *Phase Trans.* **79**, 1043 (2006).
- ¹²Y. Yang, L. G. Bai, K. Zhu, Y. L. Liu, S. Jiang, J. Liu, J. Chen, and X. R. Xing, *J. Phys.: Condens. Matter* **21**, 385901 (2009).
- ¹³A. G. Gavriliuk, I. S. Lyubutin, and V. V. Struzhkin, *JETP Lett.* **86**, 532 (2007).
- ¹⁴A. G. Gavriliuk, V. V. Struzhkin, I. S. Lyubutin, M. Y. Hu, and H. K. Mao, *JETP Lett.* **82**, 224 (2005).
- ¹⁵I. S. Lyubutin, A. G. Gavriliuk, and V. V. Struzhkin, *JETP Lett.* **88**, 524 (2008).
- ¹⁶I. S. Lyubutin, S. G. Ovchinnikov, A. G. Gavriliuk, and V. V. Struzhkin, *Phys. Rev. B* **79**, 085125 (2009).
- ¹⁷A. G. Gavriliuk, V. V. Struzhkin, I. S. Lyubutin, and I. A. Troyan, *JETP Lett.* **86**, 197 (2007).
- ¹⁸A. A. Belik, H. Yusa, N. Hirao, Y. Ohishi, and E. T. Muromachi, *Chem. Mater.* **21**, 3400 (2009).
- ¹⁹R. Haumont, P. Bouvier, A. Pashkin, K. Rabia, S. Frank, B. Dkhil, W. A. Crichton, C. A. Kuntscher, and J. Kreisel, *Phys. Rev. B* **79**, 184110 (2009).
- ²⁰D. P. Kozlenko, A. A. Belik, A. V. Belushkin, E. V. Lukin, W. G. Marshall, B. N. Savenko, and E. Takayama-Muromachi, *Phys. Rev. B* **84**, 094108 (2011).
- ²¹H. K. Mao, P. M. Bell, J. W. Shaner, and D. J. Steinberg, *J. Appl. Phys.* **49**, 3276 (1978).
- ²²J. D. Bucci, B. K. Robertson, and W. J. James, *J. Appl. Crystallogr.* **5**, 187 (1972).
- ²³S. Karimi, I. M. Reaney, Y. Han, J. Pokorny, and I. Sterianou, *J. Mater. Sci.* **44**, 5102 (2009).
- ²⁴F. Kubel and H. Schmid, *Acta Crystallogr. B* **46**, 698 (1990).
- ²⁵A. M. Glazer, *Acta Crystallogr. B* **28**, 3384 (1972).
- ²⁶R. Haumont, J. Kreisel, P. Bouvier, and F. Hippert, *Phys. Rev. B* **73**, 132101 (2006).
- ²⁷R. Haumont, R. Saint-Martin, and C. Byl, *Phase Trans.* **81**, 881 (2008).
- ²⁸M. N. Iliev, M. V. Abrashev, H.-G. Lee, V. N. Popov, Y. Y. Sun, C. Thomsen, R. L. Meng, and C. W. Chu, *Phys. Rev. B* **57**, 2872 (1998).
- ²⁹M. K. Singh and H. M. Jang, *Appl. Phys. Lett.* **88**, 042907 (2006).
- ³⁰J. Hlinka, J. Pokorny, S. Karimi, and I. M. Reaney, *Phys. Rev. B* **83**, 020101(R) (2011).
- ³¹Y. J. Wu, X. K. Chen, J. Zhang, and X. J. Chen, *Physica B* **411**, 106 (2013).
- ³²H. Yusa, A. A. Belik, E. T. Muromachi, N. Hirao, and Y. Ohishi, *Phys. Rev. B* **80**, 214103 (2009).
- ³³I. A. Kornev, L. Bellaiche, P. Bouvier, P.-E. Janolin, B. Dkhil, and J. Kreisel, *Phys. Rev. Lett.* **95**, 196804 (2005).
- ³⁴Z. Wu and R. E. Cohen, *Phys. Rev. Lett.* **95**, 037601 (2005).
- ³⁵M. Ahart, M. Somayazulu, P. Dera, H.-K. Mao, R. E. Cohen, R. J. Hemley, R. Yang, and Z. Wu, *Nature* **451**, 545 (2008).